Inverse Problems in Imaging: a Hyperprior Bayesian Approach

Cecilia Aguerrebere, Andrés Almansa, Julie Delon, Yann Gousseau, Pablo Musé

Inverse Problems in Imaging: a Hyperprior Bayesian Approach

Cecilia Aguerrebere, Andrés Almansa, Julie Delon, Yann Gousseau and Pablo Musé

***Abstract*—Patch models have proven successful to solve a variety of inverse problems in image restoration. Recent methods, combining Gaussian patch models with a Bayesian approach, achieve state-of-the-art results in several restoration problems. Different strategies are followed to define and estimate the patch models. In particular, a fixed model can be used for all image patches, or the model can be estimated locally for each patch. Per-patch model estimation has proven very powerful for image denoising, but it becomes seriously ill-posed for other inverse problems such as the interpolation of random missing pixels or zooming. In this work, we present a new framework for image restoration that makes it possible to use per-patch priors for these more general inverse problems. To this aim, we make use of a hyperprior on the model parameters which overcomes the ill-posedness of the per-patch estimation. We also make this framework general enough to include realistic additive noise models. This yields state-of-the-art results in problems such as interpolation, denoising and zooming. Moreover, taking advantage of the generality of the framework, we present an application to the generation of high dynamic range images from a single snapshot. Experiments conducted on synthetic and real data show the effectiveness of the proposed approach.**

***Index Terms*—Non-local patch-based restoration, Bayesian restoration, Maximum a Posteriori, Gaussian Mixture Models, hyper-prior, conjugate distributions, high dynamic range imaging, single shot HDR.**

I. Introduction

DIGITAL images are subject to a wide variety of degradations, which in most cases can be modeled as

$$\mathrm{Z} = \boldsymbol{D}\mathrm{C} + \mathrm{N}, \tag{1}$$

where Z is the observation, $\boldsymbol{D}$ is the degradation operator, C is the underlying ground-truth image and N is additive noise. Different settings of the degradation matrix $\boldsymbol{D}$ model different problems such as zooming, deblurring or random missing pixels. Different characterizations of the noise term N describe noise degradations, ranging from the classical additive Gaussian noise to more complicated and realistic models such as multiplicative or signal dependent noise. These degradations are often combined in practice. For instance, raw images captured with regular digital cameras combine signal dependent noise, limited spatial resolution and limited dynamic range, among other problems [1].

Inspired by the patch-based approach for texture synthesis proposed by Efros and Leung [2], Buades et al. [3] introduced the use of patches and the self-similarity hypothesis to the denoising problem leading to a new era of patch-based image restoration techniques. A major step forward in fully exploiting the potential of patches was taken with the introduction of patch prior models. Recent state-of-the-art methods make use of patch models in a Bayesian framework to restore degraded images. Some of them are devoted to the denoising problem [4], [5], [6], [7], while others propose a more general framework for the solution of image inverse problems [8], [9], including for instance inpainting, deblurring and zooming. The work by Lebrun et al. [10], [6] presents a thorough analysis of several recent restoration methods, revealing their common roots and their relationship with the Bayesian approach.

Among the state-of-the-art restoration methods, two noticeable approaches are the patch-based Bayesian approach by Yu et al. [9], namely the piece-wise linear estimators (PLE), and the non-local Bayes (NLB) algorithm by Lebrun et al. [6]. PLE is a general framework for the solution of image inverse problems under Model (1), while NLB is a denoising method ($\boldsymbol{D} = Id$). Both methods use a Gaussian patch prior learnt from image patches through iterative procedures. In the case of PLE, patches are modeled according to a Gaussian Mixture Model (GMM), with a relatively small number of classes (19 in all their experiments), whose parameters are learnt from all image patches.[1] In the case of NLB, each patch is associated with a single Gaussian model, whose parameters are computed from similar patches chosen from a local neighborhood, i.e., a search window centered at the patch, so the number of classes is not chosen a priori (one class per patch). We refer hereafter to this kind of patch model as *local*, because it gives a different model per-patch and it is computed from similar patches in a local neighborhood, as opposed to the GMM that uses a fixed number of classes to represent all patches.

NLB outperforms PLE in the denoising task [11], mostly due to its local model estimation. Nevertheless, PLE obtains state-of-the-art results in other applications such as interpolation of missing pixels, deblurring and zooming. In particular, PLE yields very good results in interpolation of random missing pixels with high masking rates. A variant of PLE for inpainting is proposed by Wang [12] (E-PLE), using a GMM initialized from natural images instead of using synthetic

C. Aguerrebere is with the Department of Electrical and Computer Engineering, Duke University, Durham NC 27708, US (e-mail: cecilia.aguerrebere@duke.edu)

A. Almansa and Y. Gousseau are with the LTCI CNRS, Télécom ParisTech, Université Paris-Saclay, 75013 Paris, France (e-mail: gousseau,almansa@telecom-paristech.fr).

J. Delon is with MAP5 (CNRS UMR 8145), Université Paris Descartes, 75270 Paris Cedex 06 (e-mail: julie.delon@parisdescartes.fr)

P. Musé is with the Department of Electrical Engineering, Universidad de la República, 11300 Montevideo, Uruguay (e-mail: pmuse@fing.edu.uy)

[1] Actually, the authors report the use of 128×128 image sub-regions in their experiments, so we may consider PLE as a semi-local approach.

images of edges as it is done in PLE.

Zoran and Weiss [8] (EPLL) follow a similar approach, but instead of iteratively updating the GMM from image patches, they use a larger number of classes (200) that are fixed and learnt from a large database of natural image patches (2×10^6 patches). Wang and Morel [7] claim that, in the case of denoising, it is better to have fewer models that are updated with the image patches (as in PLE) than having a large number of fixed models (as in EPLL). Moreover, unlike the previous methods, EPLL restores image patches according to the GMM prior[2] while keeping the restored image close to the corrupted image for a given corruption model.

All of the previous restoration approaches share a common Bayesian framework based on Gaussian patch priors. As said above, relying on local priors [6], [7] has proven more accurate for the task of image denoising than relying on a limited number of Gaussian models [8], [9]. However, such local priors are very difficult to estimate for more general restoration problems, especially when the image degradations involve missing pixels. The main contribution of this work is to propose a robust framework enabling the use of such Gaussian local priors for solving general restoration problems, by drawing on what is known in Bayesian statistics as a hyperprior.

We propose to model image patches according to a Gaussian prior, whose parameters will be estimated locally from similar patches. The main challenge with this framework is to estimate the Gaussian parameters, i.e. the mean μ and the covariance matrix $\mathbf{\Sigma}$, from a set of patches with potentially high degradation levels. For example, in the case of the interpolation of random missing pixels with a masking rate of 70%, the patches used for the estimation of μ and $\mathbf{\Sigma}$ will lack 70% of the pixels, thus making the estimation problem very ill-posed. In order to tackle this problem, we include prior knowledge on the model parameters making use of a hyperprior, i.e. a probability distribution on the parameters of the prior. In Bayesian statistics, μ and $\mathbf{\Sigma}$ are known as hyperparameters, since they are the parameters of a prior distribution, while the prior on them is called a hyperprior. The use of a hyperprior allows to estimate μ and $\mathbf{\Sigma}$ from similar patches even if they present high degradation levels. The information provided by the hyperprior compensates for the patches missing information.

Image patches are then restored using the maximum a posteriori (MAP) estimator with the computed Gaussian model. Experiments conducted on both synthetic and real data show state-of-the-art results obtained by the proposed approach in various problems such as interpolation, denoising and zooming.

This general framework is also applied to the generation of high dynamic range (HDR) images. Due to physical limitations, current digital sensors cannot capture faithful representations of HDR scenes. HDR imaging tackles this problem and seeks to accurately capture and represent scenes with the largest possible irradiance range. As will be detailed in Section V, HDR imaging can be achieved from a single snapshot using specially modified sensors. We propose here a novel approach to single shot HDR imaging using the proposed restoration framework. This simple, yet powerful, approach shows excellent performance in several examples both on synthetic and real data.

[2]EPLL does not impose a given prior, GMM is an option among others.

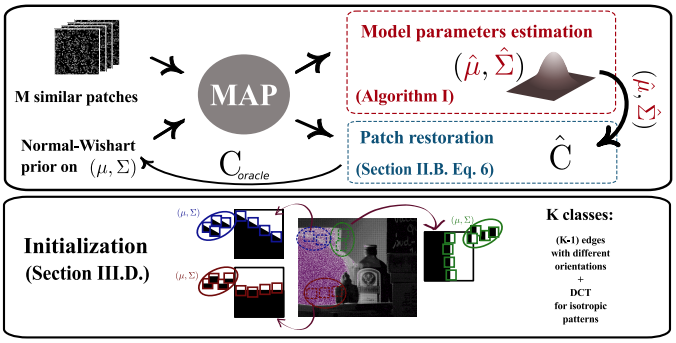

Fig. 1. Diagram of the proposed iterative approach with the corresponding initialization stage.

The article is organized as follows. Section II introduces the proposed approach while Section III presents the main implementation aspects. Supportive experiments are presented in Section IV. Section V is devoted to the application of the proposed framework to the HDR imaging problem. Last, conclusions are summarized in Section VI.

II. Hyperprior Bayesian Estimator

We describe here the proposed restoration method, called Hyperprior Bayesian Estimator (HBE). Following the idea of the recent Bayesian approach [6], we assume a Gaussian prior for image patches whose parameters μ and $\mathbf{\Sigma}$ are estimated from a group of patches similar to the current patch. The particularity of our method is that it uses a joint maximum a posteriori formulation to estimate both the image patches and the parameters μ and $\mathbf{\Sigma}$, thanks to a Bayesian hyperprior model on these parameters. The maximization alternates two steps : first the log-likelihood is maximized in μ and $\mathbf{\Sigma}$ by combining similar patches and the hyperprior on them, and then the patch is restored under the Gaussian prior defined by μ and $\mathbf{\Sigma}$. Figure 1 shows a diagram of the proposed iterative approach.

A. Patch degradation model

The observed image z is decomposed into I overlapping patches $\{\mathrm{z}_i\}_{i=1,\dots,I}$ of size $\sqrt{n} \times \sqrt{n}$. Each patch $\mathrm{z}_i \in \mathbb{R}^{n \times 1}$ is considered to be a realization of the random variable Z_i given by

$$\mathrm{Z}_i = \boldsymbol{D}_i \mathrm{C}_i + \mathrm{N}_i, \tag{2}$$

where $\boldsymbol{D}_i \in \mathbb{R}^{n \times n}$ is a degradation operator, $\mathrm{C}_i \in \mathbb{R}^{n \times 1}$ is the original patch we seek to estimate and $\mathrm{N}_i \in \mathbb{R}^{n \times 1}$ is an additive noise term, not necessarily identically distributed as we will see.

In this paper, we are interested in different application scenarios, in which the degradation operator $\boldsymbol{D}_i$ (supposed to be known) can represent resolution change (zooming) or random missing pixels (inpainting). As for the noise term N_i,

we assume that it is well modeled by a Gaussian distribution $\mathrm{N}_i \sim \mathcal{N}(0, \mathbf{\Sigma}_{N_i})$. The distribution of Z_i given C_i can thus be written as

$$\begin{aligned} &p(\mathrm{Z}_i \mid \mathrm{C}_i) \sim \mathcal{N}(\boldsymbol{D}_i\mathrm{C}_i, \mathbf{\Sigma}_{N_i}) \\ &\propto |\mathbf{\Sigma}_{N_i}^{-1}|^{\frac{1}{2}} \exp\left(-\frac{1}{2}(\mathrm{Z}_i - \boldsymbol{D}_i\mathrm{C}_i)^T\mathbf{\Sigma}_{N_i}^{-1}(\mathrm{Z}_i - \boldsymbol{D}_i\mathrm{C}_i)\right). \end{aligned} \tag{3}$$

In this noise model, the matrix $\mathbf{\Sigma}_{N_i}$ is only assumed to be diagonal (the noise is uncorrelated). It can represent a constant variance, spatially variable variances or even variances dependent on the pixel value (to approximate Poisson noise).

This degradation model is deliberately generic. We will see in Section IV that keeping a broad noise model is essential to properly tackle the problem of high dynamic range (HDR) estimation from a single image. It also includes a wide range of restoration problems generally studied in the literature, such as the particular case of multiplicative noise.

B. Joint Maximum A Posteriori

Following the direction of Bayesian patch-based methods, we assume a Gaussian prior for each patch, with unknown mean μ and covariance matrix $\mathbf{\Sigma}$

$$p(\mathrm{C} \mid \mu, \mathbf{\Sigma}) \sim \mathcal{N}(\mu, \mathbf{\Sigma}).$$

In the literature, μ and $\mathbf{\Sigma}$ are either estimated locally from a set of similar patches [6], or chosen from a finite set of precomputed parameters that are learned globally [9]. The first solution is very accurate for Gaussian denoising, but not reliable when pixels are missing. The second one is more robust but yields smoother results.

The proposed approach uses a **joint Maximum a Posteriori** (MAP) in order to estimate both the patch C and its Gaussian parameters from a set of similar patches. To this aim, we make use of a hyperprior on μ and $\mathbf{\Sigma}$. On the one hand, using similar patches gives a spatially adaptive or local characterization of the patch [6]. On the other hand, including the hyperprior makes the parameter estimation more robust, which is critical when few similar patches are available or when some pixels are unknown (e.g. for interpolation and zooming).

To simplify calculations, we work with the precision matrix $\mathbf{\Lambda} = \mathbf{\Sigma}^{-1}$ instead of the covariance matrix $\mathbf{\Sigma}$. As it is usual when considering hyperpriors, we assume that the parameters μ and $\mathbf{\Sigma}$ follow a conjugate distribution. In our case, that boils down to assuming a Normal-Wishart[3] prior for the couple $(\mu, \mathbf{\Lambda})$,

$$\begin{aligned} p(\mu, \mathbf{\Lambda}) &= \mathcal{N}(\mu|\mu_0, (\kappa\mathbf{\Lambda})^{-1})\mathcal{W}(\mathbf{\Lambda}|(\nu\mathbf{\Sigma}_0)^{-1}, \nu) \\ &\propto |\mathbf{\Lambda}|^{1/2} \exp\left(-\frac{\kappa}{2}(\mu - \mu_0)\mathbf{\Lambda}(\mu - \mu_0)^T\right) \\ &\quad |\mathbf{\Lambda}|^{(\nu-n-1)/2} \exp\left(-\frac{1}{2}\mathrm{tr}(\nu\mathbf{\Sigma}_0\mathbf{\Lambda})\right), \end{aligned} \tag{4}$$

[3]The Normal-Wishart distribution is the conjugate prior of a multivariate normal distribution with unknown mean and covariance matrix. $\mathcal{W}$ denotes the Wishart distribution [13].

where μ_0 is a prior on μ, $\mathbf{\Sigma}_0$ is a prior on $\mathbf{\Sigma}$, $\kappa > 0$ and $\nu > n - 1$ are a scale parameter and the degrees of freedom of the Normal-Wishart respectively.

Now, assume that we observe a group $\{\mathrm{Z}_i\}_{i=1,\dots,M}$ of similar patches and that we want to recover the restored patches $\{\mathrm{C}_i\}_{i=1,\dots,M}$. If these unknown $\{\mathrm{C}_i\}$ are independent and follow the same Gaussian model, we can compute the joint maximum a posteriori

$$\begin{aligned} &\underset{\{\mathrm{C}_i\},\mu,\mathbf{\Lambda}}{\arg\max}\ p(\{\mathrm{C}_i\}, \mu, \mathbf{\Lambda} \mid \{\mathrm{Z}_i\}) = \\ &\underset{\{\mathrm{C}_i\},\mu,\mathbf{\Lambda}}{\arg\max}\ p(\{\mathrm{Z}_i\} \mid \{\mathrm{C}_i\}, \mu, \mathbf{\Lambda})\ p(\{\mathrm{C}_i\} \mid \mu, \mathbf{\Lambda})\ p(\mu, \mathbf{\Lambda}) = \\ &\underset{\{\mathrm{C}_i\},\mu,\mathbf{\Lambda}}{\arg\max}\ p(\{\mathrm{Z}_i\} \mid \{\mathrm{C}_i\})\ p(\{\mathrm{C}_i\} \mid \mu, \mathbf{\Lambda})\ p(\mu, \mathbf{\Lambda}). \end{aligned} \tag{5}$$

In this product, the first term is given by the noise model (Section II-A), the second one is the Gaussian prior on the set of patches $\{\mathrm{C}_i\}$ and the third one is the hyperprior (4).

Proposition 1. *Assume that (μ, Λ) follow the Normal-Wishart distribution* (4)*, that $\mathrm{C}_1, \dots, \mathrm{C}_M|\mu, \Lambda$ are independent realizations of $\mathcal{N}(\mu, \Lambda^{-1})$, and that $\mathrm{Z}_1, \dots, \mathrm{Z}_M|\mathrm{C}_1, \dots, \mathrm{C}_M$, are independent realizations of the respective distributions $\mathcal{N}(\boldsymbol{D}_i\mathrm{C}_i, \mathbf{\Sigma}_{N_i})$. Then, under the assumption that the noise covariance matrix $\mathbf{\Sigma}_{N_i}$ is independent of C_i for each i, if the values $(\{\widehat{\mathrm{C}}_i\}, \widehat{\mu}, \widehat{\mathbf{\Lambda}})$ maximize the unified log-likelihood $\log p(\{\mathrm{C}_i\}, \mu, \mathbf{\Lambda} \mid \{\mathrm{Z}_i\})$, they must satisfy the following equations*

$$\widehat{\mathrm{C}}_i = \widehat{\mathbf{\Lambda}}^{-1}\boldsymbol{D}_i^T(\boldsymbol{D}_i\widehat{\mathbf{\Lambda}}^{-1}\boldsymbol{D}_i^T + \mathbf{\Sigma}_{N_i})^{-1}(\mathrm{Z}_i - \boldsymbol{D}_i\widehat{\mu}) + \widehat{\mu}. \tag{6}$$

$$\widehat{\mu} = \frac{M\overline{C} + \kappa\mu_0}{M + \kappa}, \quad \textit{with } \overline{C} = \frac{1}{M}\sum_{i=1}^{M}\widehat{\mathrm{C}}_i. \tag{7}$$

and

$$\widehat{\mathbf{\Lambda}}^{-1} = \frac{\nu\mathbf{\Sigma}_0 + \kappa(\widehat{\mu} - \mu_0)(\widehat{\mu} - \mu_0)^T + \sum_{i=1}^{M}(\widehat{\mathrm{C}}_i - \widehat{\mu})(\widehat{\mathrm{C}}_i - \widehat{\mu})^T}{\nu + M - n}. \tag{8}$$

Proof. See Appendix A. □

The expression of $\widehat{\mathrm{C}}_i$ in (6) is obtained under the hypothesis that the noise covariance matrix Σ_{N_i} does not depend on C_i. Observe that it can be shown that under the somewhat weaker hypothesis that the noise N_i and the signal C_i are uncorrelated, this estimator is also the affine estimator $\tilde{\mathrm{C}}_i$ that minimizes the Bayes risk $\mathbb{E}[(\tilde{\mathrm{C}}_i - \mathrm{C}_i)^2]$.

Proposition 2. *Assume that the noise has zero mean and is not correlated to the signal C_i. Then, the affine estimator $\tilde{\mathrm{C}}_i$ that minimizes the Bayes risk $\mathbb{E}[(\tilde{\mathrm{C}}_i - \mathrm{C}_i)^2]$ is given by*

$$\tilde{\mathrm{C}}_i = \widehat{\mathbf{\Lambda}}^{-1}\boldsymbol{D}_i^T(\boldsymbol{D}_i\widehat{\mathbf{\Lambda}}^{-1}\boldsymbol{D}_i^T + \mathbf{\Sigma}_{\mathrm{N}_i})^{-1}(\mathrm{Z}_i - \boldsymbol{D}_i\widehat{\mu}) + \widehat{\mu}. \tag{9}$$

Proof. See Appendix A, paragraph *(f)*. □

The uncorrelatedness of N_i and C_i is a quite reasonnable hypothesis in practice : this is for instance the case if the noise can be written as $N_i = f(C_i)\varepsilon_i$ where ε_i is independent of C_i. This includes very different noise models, including a reasonable approximation of the acquisition by a camera sensor in which the noise variance is an affine function of the signal [14].

a) Interpretation of the MAP in μ, Λ: From (7), we find that the MAP estimator of μ is a weighted average of two terms: the mean estimated from the similar restored patches and the prior μ_0. The parameter κ controls the confidence level we have on the prior μ_0. With the same idea, we observe that the MAP estimator for $\mathbf{\Lambda}$ is a combination of the covariance matrix estimated from the restored patches

$$\sum_{i=1}^{M}(\widehat{\mathrm{C}}_i - \widehat{\mu})(\widehat{\mathrm{C}}_i - \widehat{\mu})^T, \tag{10}$$

the covariance imposed by $\widehat{\mu}$ (since μ and $\mathbf{\Lambda}$ are not independent),

$$(\widehat{\mu} - \mu_0)(\widehat{\mu} - \mu_0)^T, \tag{11}$$

and the prior on $\mathbf{\Lambda}$ (or equivalently on $\mathbf{\Sigma}^{-1}$),

$$\mathbf{\Sigma}_0^{-1}. \tag{12}$$

If we inject expression (6) into the previous expressions of $\widehat{\mu}$ and $\widehat{\mathbf{\Lambda}}$, we obtain

$$\widehat{\mu} = (\kappa \mathrm{Id} + \sum_{i=1}^{M} A_i \boldsymbol{D}_i)^{-1}(\sum_{i=1}^{M} A_i \mathrm{Z}_i + \kappa\mu_0), \tag{13}$$

and

$$\widehat{\mathbf{\Lambda}}^{-1} = \frac{\nu\mathbf{\Sigma}_0 + \kappa(\widehat{\mu} - \mu_0)(\widehat{\mu} - \mu_0)^T + \sum_{i=1}^{M} A_i(\mathrm{Z}_i - \boldsymbol{D}_i\widehat{\mu})(\mathrm{Z}_i - \boldsymbol{D}_i\widehat{\mu})^T A_i^T}{\nu + M - n} \tag{14}$$

with $A_i = \widehat{\mathbf{\Lambda}}^{-1}\boldsymbol{D}_i^T(\boldsymbol{D}_i\widehat{\mathbf{\Lambda}}^{-1}\boldsymbol{D}_i^T + \mathbf{\Sigma}_{N_i})^{-1}$.

b) Practical estimation: Since (13) depends on $\mathbf{\Lambda}$ and (14) depends on μ and $\mathbf{\Lambda}$, these are not closed-forms formulas for the estimators. Hence, we propose to use an iterative approach to compute the parameters, as summarized in Algorithm 1. This algorithm results from the combination of two procedures. The outer loop follows from the classic EM estimation procedure for the mean and covariance (or precision) matrix. The inner one, which deals with the estimation of the precision matrix, converges if and only if the spectral norm of the precision matrix is less than one. In case this condition on the spectral norm of $\mathbf{\Lambda}$ holds, since EM and therefore the posteriors are guaranteed to converge to a local maximum, μ and $\mathbf{\Lambda}$ are ensured to converge to local maximizers. In practice, we observe that the algorithm converges after a single iteration of the outer loop with 3 to 4 iterations of the inner loop.

C. Summary of the proposed algorithm

The analysis previously presented leads to an iterative algorithm that implements the proposed approach. Two stages are alternated: the restoration step, where all patches are reconstructed, and the model estimation step, where the model parameters are updated (Figure 1). For the model estimation step, the result of the previous iteration is used as an "*oracle*". In practice, the algorithm is found to converge after 3 to 4 iterations. The procedure is summarized in Algorithm 2.

Algorithm 1: Computation of $\hat{\mu}$ and $\hat{\mathbf{\Lambda}}$.

Input: Z, $\boldsymbol{D}$, $\mu_0, \mathbf{\Sigma}_0, \kappa, \nu$ (see details in Section III-C)
Output: $\hat{\mu}$, $\hat{\mathbf{\Lambda}}$
Initialization: Set $\mathbf{\Lambda} = \mathbf{\Sigma}_0^{-1}$
for *it = 1 to maxIts*$_0$ **do**
  Compute $\hat{\mu}$ according to (13)
  Set $\mu = \hat{\mu}$.
  for *it = 1 to maxIts*$_1$ **do**
    Compute $\hat{\mathbf{\Lambda}}$ according to (14).
    Set $\mathbf{\Lambda} = \hat{\mathbf{\Lambda}}$.
  end
end

III. Implementation details

A. Search for similar patches

The similar patches are all patches within a window search centered at the current patch, that have L_2 distance to it below a given threshold. This threshold is given by a tolerance parameter times the distance to the nearest neighbor. The patch comparison is performed in an oracle image (i.e. the result of the previous iteration), so all pixels are known. However, it may be useful to assign different confidence levels to the known pixels and to those originally missing and then restored. For all the experimental results presented in Section IV, the distance between patches c_p and c_q in the oracle image C_{oracle} is computed according to

$$d(p,q) = \frac{\sum_{j=1}^{N}(\mathrm{c}_p^j - \mathrm{c}_q^j)^2\omega_{p,q}^j}{\sum_{j=1}^{N}\omega_{p,q}^j}, \tag{15}$$

where j indexes the pixels in the patch, $\omega_{p,q}^j = 1$ if $\boldsymbol{D}_p^j = \boldsymbol{D}_q^j = 1$ (known pixel) and $\omega_{p,q}^j = 0.01$ otherwise (originally missing then restored pixel) [15]. With this formulation, known pixels are assigned a much higher priority than unknown ones. Variations of these weights could be explored.

B. Collaborative Filtering

The proposed method computes one Gaussian model per image patch according to Equations (13) and (14). In order to reduce the computational cost, we rely on the collaborative filtering idea previously introduced for patch-based denoising techniques [6], [16]. Based on the hypothesis that similar patches share the same model, instead of computing a different pair $(\mu, \mathbf{\Sigma})$ for each patch, we assign the same model to all patches in the set of similar patches. The restoration is thus performed for all similar patches according to the computed model.

C. Parameters setting

The four parameters of the Normal-Wishart distribution: κ, ν, the prior mean μ_0 and the prior covariance matrix $\mathbf{\Sigma}_0$, must be set in order to compute μ and $\mathbf{\Sigma}$ using (13) and (14).

c) Choice of κ and ν: The computation of μ according to (13) combines the mean $\sum_{i=1}^{M} A_i \mathrm{Z}_i$ estimated from the similar patches and the prior mean μ_0. The parameter κ is related to the degree of confidence we have in the prior μ_0. Hence, its value should be a trade-off between the confidence we have in the prior accuracy vs. the one we have in the information provided by the similar patches. The latter improves when both M (*i.e.* the number of similar patches) and $P = \mathrm{trace}(D_i)$ (*i.e.* the number of known pixels in the current patch) increase. These intuitive insights suggest the following rule to choose the value of κ:

$$\kappa = M\alpha, \quad \alpha = \begin{cases} \alpha_L & \text{if } P \text{ and } M > \text{threshold} \\ \alpha_H & \text{otherwise.} \end{cases} \tag{16}$$

A similar reasoning leads to the same rule for ν,

$$\nu = M\alpha + n \tag{17}$$

where the addition of n ensures the condition $\nu > n - 1$ required by the Normal-Wishart prior to be verified.

This rule is used to obtain the experimental results presented in Section IV, and proved to be a consistently good choice despite its simplicity. However, setting these parameters in a more general setting is not a trivial task and should be the subject of further study. In particular we could explore a more continuous dependence of α on P, M, and possibly a third term $Q = \sum_{i=1}^{n} S_{ii}$ where $S = \sum_{j=1}^{M} \mathbf{\Lambda}^{-1} \boldsymbol{D}_j \mathbf{\Lambda}_j^* \boldsymbol{D}_j$. This third term Q estimates to what an extent similar patches cover the missing pixels in the current patch.

Algorithm 2: Summary of the proposed algorithm.

Input: Z, $\boldsymbol{D}$, $\mu_0, \mathbf{\Sigma}_0, \kappa, \nu$ (see details in Section III-C)
Output: $\tilde{\mathrm{C}}$

```
Decompose Z and D into overlapping patches.
Initialization: Compute first oracle image C_oracle (see details in Section III-D)
for it = 1 to maxIts_2 do
    for all patches not yet restored do
        Find patches similar (L^2 distance) to the current z_i in C_oracle (see details in Section III-A).
        Compute μ_0 and Σ_0 from C_oracle (see details in Section III-C).
        Compute μ̂ and Σ̂ following Algorithm 1.
        Restore the similar patches using (6) (see details in Section III-B).
    end
    Perform aggregation to restore the image.
    Set C_oracle = C̃.
end
```

d) Setting of μ_0 and $\mathbf{\Sigma}_0$: Assuming an oracle image C_{oracle} is available (see details in Section II-C), μ_0 and $\mathbf{\Sigma}_0$ can be computed using the classical MLE estimators from a set of similar patches $(\tilde{\mathrm{c}}_1, \ldots, \tilde{\mathrm{c}}_M)$ taken from C_{oracle}

$$\mu_0 = \frac{1}{M} \sum_{j=1}^{M} \tilde{\mathrm{c}}_j, \quad \mathbf{\Sigma}_0 = \frac{1}{M-1} \sum_{j=1}^{M} (\tilde{\mathrm{c}}_j - \mu_0)(\tilde{\mathrm{c}}_j - \mu_0)^T. \tag{18}$$

This is the same approach followed by Lebrun et al. [6] to estimate the patch model parameters in the case of denoising. As previously stated, the method from [6] cannot be directly applied to zooming or interpolation due to the presence of missing pixels.

D. Initialization

A good initialization is crucial since we aim at solving a non-convex problem through an iterative procedure. Yu et al. [9] propose to initialize the PLE algorithm by learning the K GMM covariance matrices from synthetic images of edges with different orientations as well as the DCT basis to represent isotropic patterns. As they state, in dictionary learning, the most prominent atoms represent local edges which are useful at representing and restoring contours. Hence, this initialization helps to correctly restore corrupted patches even in quite extreme cases.

Each covariance matrix $\mathbf{\Sigma}_k$, $k = 1, \ldots, K-1$, corresponds to one of $K-1$ orientations, uniformly sampled from directions zero to π. For a given orientation θ, a synthetic black-and-white image is generated and patches that touch the contour at different positions are randomly sampled from it. A covariance matrix is then computed from the sampled patches. The first eigenvector of the covariance matrix, which is almost constant, is replaced by a constant vector. This allows a class k of a given orientation to restore patches having different means. Up to a certain gray level difference, dark or bright edges with the same orientation are correctly represented by the same class. A Gram-Schmidt orthogonalization is computed on the other eigenvectors to ensure the orthogonality of the basis. The eigenvalues of all bases are initialized with the same values, chosen to have a fast decay. Lastly, the DCT basis is added to represent isotropic image patterns, making a total of K classes. The mean of each class μ_k, $k = 1, \ldots, K$, is initialized to zero. The authors claim that they have found in practice that $K = 19$ classes (i.e. 18 orientations, 10 degrees apart) give a correct reconstruction and are a good compromise between performance and complexity for a patch size of 8×8. The fact that the algorithm is applied in regions of size 128×128, and therefore localized, also explains why this a priori small number of classes can be suitable to describe all image patches.

To initialize the proposed algorithm, we follow the approach by Yu et al. [9] and compute the K covariance matrices $\mathbf{\Sigma}_k$ as previously described. Then, each image patch z_i is reconstructed under each class $k = 1, \ldots, K$ as

$$\tilde{\mathrm{C}}_i^k = \mathbf{\Sigma}_k \boldsymbol{D}_i^T (\boldsymbol{D}_i \mathbf{\Sigma}_k \boldsymbol{D}_i^T + \mathbf{\Sigma}_{\mathrm{N}_i})^{-1} (\mathrm{Z}_i - \boldsymbol{D}_i \mu_k) + \mu_k. \tag{19}$$

The best suited class $\tilde{k}_i$ is chosen as the one maximizing the posterior probability of the patch $p(\mathrm{C}_i | \mathrm{z}_i, \mu_k, \mathbf{\Sigma}_k)$ over k assuming $\mathrm{C} = \tilde{\mathrm{C}}_i^k$:

$$\begin{aligned} \tilde{k}_i &= \arg\max_k \log p(\mathrm{C} | \mathrm{z}_i, \mu_k, \mathbf{\Sigma}_k) \\ &= \arg\min_k \Big((\mathrm{z}_i - \boldsymbol{D}_i \tilde{\mathrm{C}}_i^k)^T \mathbf{\Sigma}_N^{-1} (\mathrm{z}_i - \boldsymbol{D}_i \tilde{\mathrm{C}}_i^k) \\ &\quad + (\tilde{\mathrm{C}}_i^k - \mu_k)^T \mathbf{\Sigma}_k^{-1} (\tilde{\mathrm{C}}_i^k - \mu_k) + \ln |\mathbf{\Sigma}_k| \Big). \end{aligned} \tag{20}$$

The first oracle is thus created by aggregating the estimations of all patches corresponding to the chosen classes. Figure 1 illustrates the proposed initialization and Algorithm 3 summarizes its steps.

Algorithm 3: Summary of the initialization procedure.

Input: Z, $\boldsymbol{D}$, K
Output: C_{oracle}
1 Decompose Z and $\boldsymbol{D}$ into overlapping patches.
2 Compute the covariance matrix of the K classes from synthetic images of edges plus the DCT.
3 Project all patches into the K classes using (19) and chose the best class using (20).
4 Compute the first oracle C_{oracle} aggregating the estimations of all patches for the chosen class.

IV. Image Restauration Experiments

In this section we illustrate the ability of the proposed method to solve several image inverse problems. Both synthetic (i.e., where we have added the degradation artificially) and real data (i.e., issued from a real acquisition process) are used. The considered problems are: interpolation, combined interpolation and denoising, denoising, and zooming. The reported values of peak signal-to-noise ratio ($PSNR = 20\log_{10}(255/\sqrt{MSE})$) are averaged over 10 realizations for each experiment (variance is below 0.1 for interpolation and below 0.05 for combined interpolation and denoising and for denoising only).

A. Synthetic degradation

e) Interpolation: Random masks with 20%, 50% and 70% of missing pixels are applied to the tested ground-truth images. The interpolation performance of the proposed method is compared to that of PLE [9], EPLL [8] and E-PLE [12] using a patch size of 8×8 for all methods. PLE parameters are set as indicated in [9] ($\sigma = 3$, $\varepsilon = 30$, $K = 19$). We used the EPLL code provided by the authors [17] with default parameters and the E-PLE code available in [12] with the parameters set as specified in this demo. The parameters for the proposed method are set to $\alpha_H = 1$, $\alpha_L = 0.5$ (α_H and α_L define the values for κ and ν, see Section III-C). The PSNR results are shown in Table I. Figure 2 shows some extracts of the obtained results, the PSNR values for the extracts and the corresponding difference images with respect to the ground-truth. The proposed method gives sharper results than the other considered methods. This is specially noticeable on the reconstruction of the texture of the fabric of Barbara's trousers shown in the first row of Figure 2 or on the strips that appear through the car's window shown in the second row of the same figure.

f) Combined interpolation and denoising: For this experiment, the ground-truth images are corrupted with additive Gaussian noise with variance 10, and a random mask with 20% and 70% of missing pixels. The parameters for all methods are set as in the previous interpolation-only experiment. Table I summarizes the PSNR values obtained by each method. Figure 3 shows some extracts of the obtained results, the PSNR values for the extracts and the corresponding difference images with respect to the ground-truth. Once again, the results show that the proposed approach outperforms the others. Fine structures, such as the mast and the ropes of the ship, as well as textures, as in Barbara's headscarf, are much better preserved (see Figure 3).

g) Denoising: For the denoising task, the proposed approach should perform very similarly to the state-of-the-art denoising algorithm NLB [6]. The following experiments are conducted in order to verify this.

The ground-truth images are corrupted with additive Gaussian noise with variance $\sigma^2 = 10, 30, 50, 80$. The code provided by the authors [18] automatically sets the NLB parameters from the input σ^2 and the patch size, in this case 8×8. For this experiment, there are no unknown pixels to interpolate (the mask $\boldsymbol{D}$ is the identity matrix).

The results of both methods are very similar if HBE is initialized with the output of the first step of NLB [6] (instead of using the initialization described in Section II-C) and the parameters κ and ν are large enough. In this case, μ_0 and $\boldsymbol{\Sigma}_0$ are prioritized in equations (13) and (14) and both algorithms are almost the same. That is what we observe in practice with $\alpha_H = \alpha_L = 100$, as demonstrated in the results summarized in Table I. The denoising performance of HBE is degraded for small κ and ν values. The reason for this is that μ_0 and $\boldsymbol{\Sigma}_0$, as well as μ and $\boldsymbol{\Sigma}$ in NLB, are computed from an oracle image resulting from the first restoration step. This restoration includes not only the denoising of each patch, but also an aggregation step that highly improves the final result. Therefore, the contribution of the first term of (13) to the computation of $\hat{\mu}$ degrades the result compared to that of using μ_0 only (i.e. using a large κ).

h) Zooming: In order to evaluate the zooming capacity of the proposed approach, ground-truth images are downsampled by a factor 2 (no anti-aliasing filter is used) and the zooming is compared to the ground-truth. The results are compared with PLE, EPLL, E-PLE and the Lanczos interpolation. Figure 4 shows extracts from the obtained results, the PSNR values for the extracts and the corresponding difference images with respect to the ground-truth. HBE yields a sharper reconstruction than the other methods.

B. Real data

For this experiment, we use raw images captured with a Canon 400D camera (set to ISO 400 and exposure time 1/160 seconds). The main noise sources for CMOS sensors are: the Poisson photon shot noise, which can be approximated by a Gaussian distribution with equal mean and variance; the thermally generated readout noise, which is modeled as an additive Gaussian distributed noise and the spatially varying gain given by the photo response non uniformity (PRNU) [14], [19]. We thus consider in this case the following noise model for the non saturated raw pixel value $\mathrm{Z}(p)$ at position p

$$\mathrm{Z}(p) \sim \mathcal{N}(g a_p \tau \mathrm{C}(p) + \mu_R, g^2 a_p \tau \mathrm{C}(p) + \sigma_R^2), \qquad (21)$$

		PSNR (dB)											
		HBE	PLE	EPLL	E-PLE	HBE	PLE	EPLL	E-PLE	HBE	PLE	EPLL	E-PLE
	% missing pixels	20%				50%				70%			
Interpolation	barbara	**45.57**	43.48	40.89	43.75	**39.11**	36.93	32.99	35.43	**34.69**	32.50	27.96	28.77
	boat	**41.43**	40.37	40.17	40.32	**34.92**	34.32	34.21	33.59	**31.37**	30.74	30.38	30.26
	traffic	35.66	35.53	**35.71**	35.10	30.17	30.12	**30.19**	28.86	**27.27**	27.12	27.13	26.64
Interpolation & Denoising	barbara	38.35	**38.37**	37.32	37.26	-	-	-	-	**33.34**	31.99	27.63	27.75
	boat	36.99	**37.02**	37.00	36.26	-	-	-	-	**30.61**	30.41	30.15	29.54
	traffic	34.07	34.13	**34.33**	33.50	-	-	-	-	26.99	26.98	**27.05**	26.35
	σ^2	HBE	NLB 10	EPLL	HBE	NLB 30	EPLL	HBE	NLB 50	EPLL	HBE	NLB 80	EPLL
Denoising	barbara	**41.26**	41.20	40.56	**38.40**	38.26	37.32	**37.13**	36.94	35.84	**35.96**	35.73	34.51
	boat	**40.05**	39.99	39.47	36.71	**36.76**	36.34	35.41	**35.46**	35.13	**34.30**	34.33	34.12
	traffic	40.73	**40.74**	40.55	**37.03**	36.99	36.86	**35.32**	35.26	35.20	**33.78**	33.70	33.72

TABLE I

RESULTS OF THE INTERPOLATION, COMBINED INTERPOLATION AND DENOISING AND DENOISING TESTS DESCRIBED IN SECTION IV-A. PATCH SIZE OF 8×8 FOR ALL METHODS IN ALL TESTS. PARAMETER SETTING FOR INTERPOLATION AND COMBINED INTERPOLATION AND DENOISING, HBE: $\alpha_H = 1$, $\alpha_L = 0.5$, PLE: $\sigma = 3$, $\varepsilon = 30$, $K = 19$ [9], EPLL: DEFAULT PARAMETERS [17], E-PLE: PARAMETERS SET AS SPECIFIED IN [12]. PARAMETER SETTING FOR DENOISING, HBE: $\alpha_H = \alpha_L = 100$, NLB: CODE PROVIDED BY THE AUTHORS [18] AUTOMATICALLY SETS PARAMETERS FROM INPUT σ^2, EPLL: DEFAULT PARAMETERS FOR THE DENOISING EXAMPLE [17]

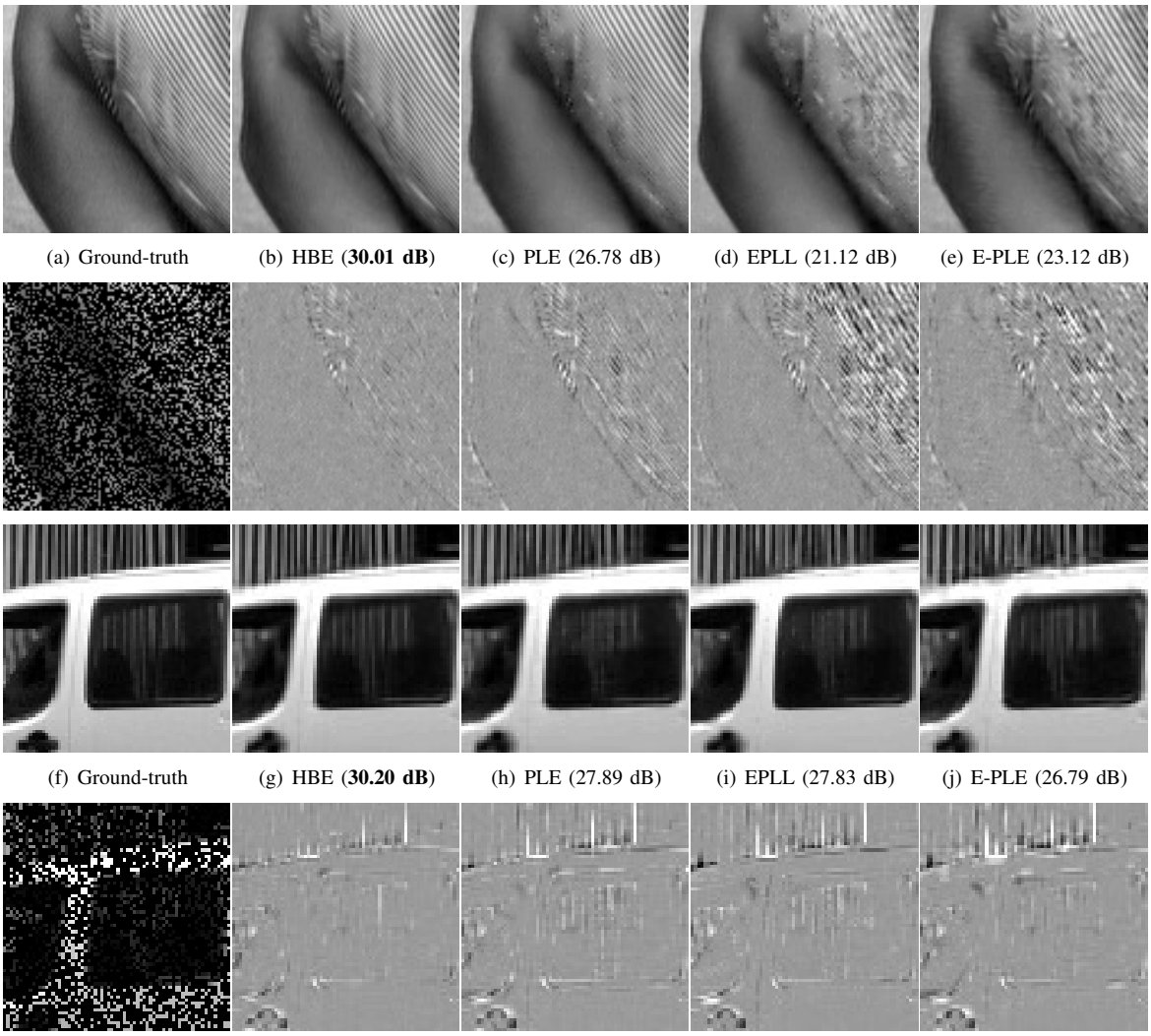

(a) Ground-truth (b) HBE (**30.01 dB**) (c) PLE (26.78 dB) (d) EPLL (21.12 dB) (e) E-PLE (23.12 dB)

(f) Ground-truth (g) HBE (**30.20 dB**) (h) PLE (27.89 dB) (i) EPLL (27.83 dB) (j) E-PLE (26.79 dB)

Fig. 2. **Synthetic data. Interpolation with 70% of randomly missing pixels**. **Left to right:** (first row) Ground-truth (extract of barbara), result by HBE, PLE, EPLL, E-PLE. (second row) input image, difference with respect to the ground-truth of each of the corresponding results. (third and fourth row) Idem for an extract of the traffic image. See Table I for the PSNR results for the complete images. Please see the digital copy for better details reproduction.

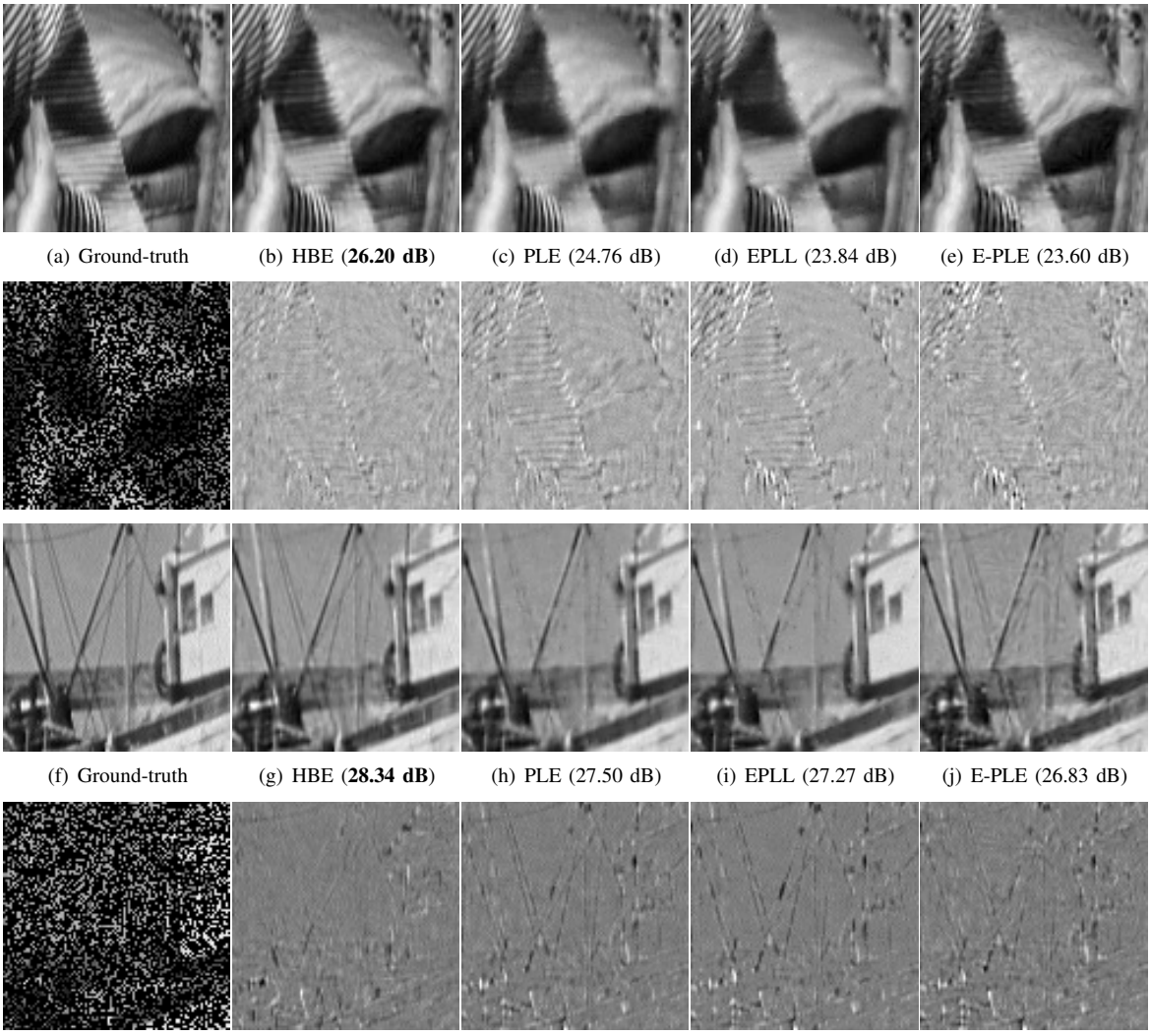

(a) Ground-truth (b) HBE (**26.20 dB**) (c) PLE (24.76 dB) (d) EPLL (23.84 dB) (e) E-PLE (23.60 dB)

(f) Ground-truth (g) HBE (**28.34 dB**) (h) PLE (27.50 dB) (i) EPLL (27.27 dB) (j) E-PLE (26.83 dB)

Fig. 3. **Synthetic data. Combined interpolation and denoising with 70% of randomly missing pixels and additive Gaussian noise** ($\sigma^2 = 10$). **Left to right:** (first row) Ground-truth (extract of barbara), result by HBE, PLE, EPLL, E-PLE. (second row) input image, difference with respect to the ground-truth of each of the corresponding results. (third and fourth row) Idem for an extract of the boat image. See Table I for the PSNR results for the complete images. Please see the digital copy for better details reproduction.

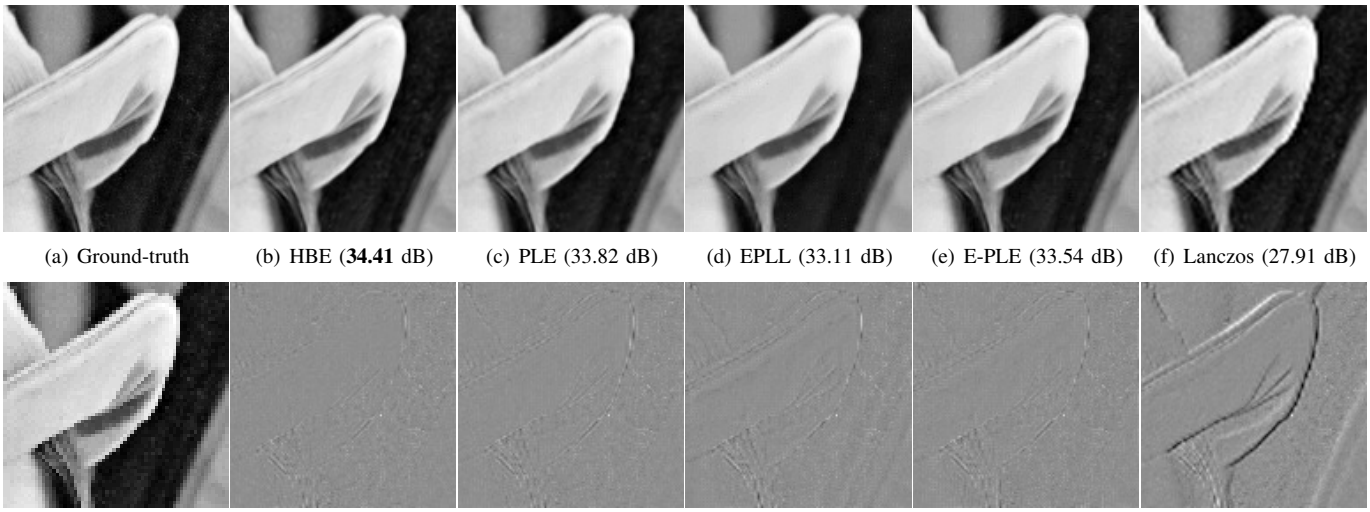

(a) Ground-truth (b) HBE (**34.41** dB) (c) PLE (33.82 dB) (d) EPLL (33.11 dB) (e) E-PLE (33.54 dB) (f) Lanczos (27.91 dB)

Fig. 4. **Synthetic data. Zooming** $\times 2$**. Left to right:** (first row) Ground-truth high resolution image (extract of lena). Result by HBE, PLE, EPLL, E-PLE, lanczos interpolation. (second row) Input low-resolution image, difference with respect to the ground-truth of each of the corresponding results. Please see the digital copy for better details reproduction.

Fig. 5. **Left. Real data.** JPEG version of the raw image used in the experiments presented in Section IV-B. The boxes show the extracts displayed in Figure 6. **Right. Synthetic data.** Ground-truth images used in the experiments presented in Section IV-A.

where g is the camera gain, a_p models the PRNU factor, τ is the exposure time, $\mathrm{C}(p)$ is the irradiance reaching pixel p, μ_R and σ_R^2 are the readout noise mean and variance. The camera parameters have to be estimated by a calibration procedure [14]. The noise covariance matrix $\mathbf{\Sigma}_N$ is thus diagonal with entries that depend on the pixel value $(\mathbf{\Sigma}_N)_p = g^2 a_p \tau \mathrm{C}(p) + \sigma_R^2$.

In order to evaluate the interpolation capacity of the proposed approach, we consider the pixels of the green channel only (i.e. 50% of the pixels in the RGGB Bayer pattern) and interpolate the missing values. We compare the results to those obtained using an adaptation of PLE to images degraded with noise with variable variance (PLEV) [20]. The results for the EPLL and E-PLE methods are not presented here since these methods are not suited for this kind of noise. Figure 6 shows extracts of the obtained results (see Figure 5 for a JPEG version of the raw image showing the location of the the extracts). As it was already observed in the synthetic data experiments, fine details and edges are better preserved. Compare for example the reconstruction of the balcony edges and the wall structure in the first row of Figure 6, as well as the structure of the roof and the railing in the second row of the same image.

C. Discussion

In all the tested examples, the results obtained by HBE for every considered inverse problem outperform or are very close to those obtained by the other evaluated methods. Details are better reconstructed and the resulting images are more sharp both in the synthetic and real data examples. The improvement is more noticeable when comparing the difference images (available for the synthetic tests only), which present less structure in the result obtained by HBE.

Even if the PLE method can be considered as semi-local (since it is applied in 128×128 regions [9]), we find that in some cases, 19 classes are not enough to correctly represent certain image patches. This is mostly the case for patches that seldom appear in the image, such as certain edges or particular textures that appear in a few patches. This is quite noticeable in the extract of Barbara's trousers and in the interior of the car (Figure 2). The specific characteristics of these patches are buried in the PLE class update when combined with many other different patches.

A local model estimation as the one performed by HBE correctly handles those cases. The performance difference is much more remarkable for the higher masking rates. In those cases, two phenomena take place. On the one hand, very few pixels are known thus making the model selection less robust. On the other hand, the model accuracy is critical since a much larger part of the patch is to be restored. The proposed method tackles the model selection problem by limiting the model estimation to similar patches found on a local search window. It has been widely observed in denoising techniques based on the self-similarity principle [21] that performance improves when restricting the patch search space to a local search window instead of using the whole image. This strategy, in addition to the hypothesis of self-similarity in that neighborhood, restricts the possible models robustifying the model estimation, which is crucial for high masking rates. Furthermore, the local model estimation, previously proven successful at describing patches [6], gives a better reconstruction even when a very large part of the patch is missing.

EPLL uses more mixture components in its GMM model than PLE, where 200 components are learnt from 2×10^6 patches of natural images [8]. The results obtained by this approach, despite using a larger number of GMM components, are not very good for the restoration of certain patches. As previously mentioned, Wang and Morel [7] claim that in the case of denoising, it is better to have fewer models that are updated with the image patches (as in PLE) rather than having a large number of fixed models (as in EPLL). In this work, we observe that the proposed approach outperforms EPLL, not only in denoising, but also in inpainting and zooming. However, here it is harder to tell if the improvement is due to the local model estimation performed from the similar patches or if it is due to the different restoration strategies followed by these methods.

V. High dynamic range imaging from a single snapshot

In this section, we propose a novel approach to generate high dynamic range (HDR) images from a single shot based on the general framework introduced in Section II.

HDR imaging aims at reproducing an extended dynamic range of luminosity compared to what can be captured using a standard digital camera. The range of luminosity which a standard digital camera can capture is often not enough to produce a faithful representation of real scenes. In the case of a static scene and a static camera, the combination of multiple images with different exposure levels is a simple and efficient solution [22], [23]. However, several problems arise when either the camera or the elements in the scene move [24], [25].

An alternative to the HDR from multiple frames was introduced by Nayar and Mitsunaga in [26]. They proposed to perform HDR imaging from a single image using spatially varying pixel exposures (SVE). An optical mask with spatially varying transmittance (see Figure 7) is placed adjacent to a conventional image sensor, thus controlling the amount of light that reaches each pixel. This gives different exposure levels to the pixels allowing a single shot to capture an increased dynamic range compared to that of the conventional sensor.

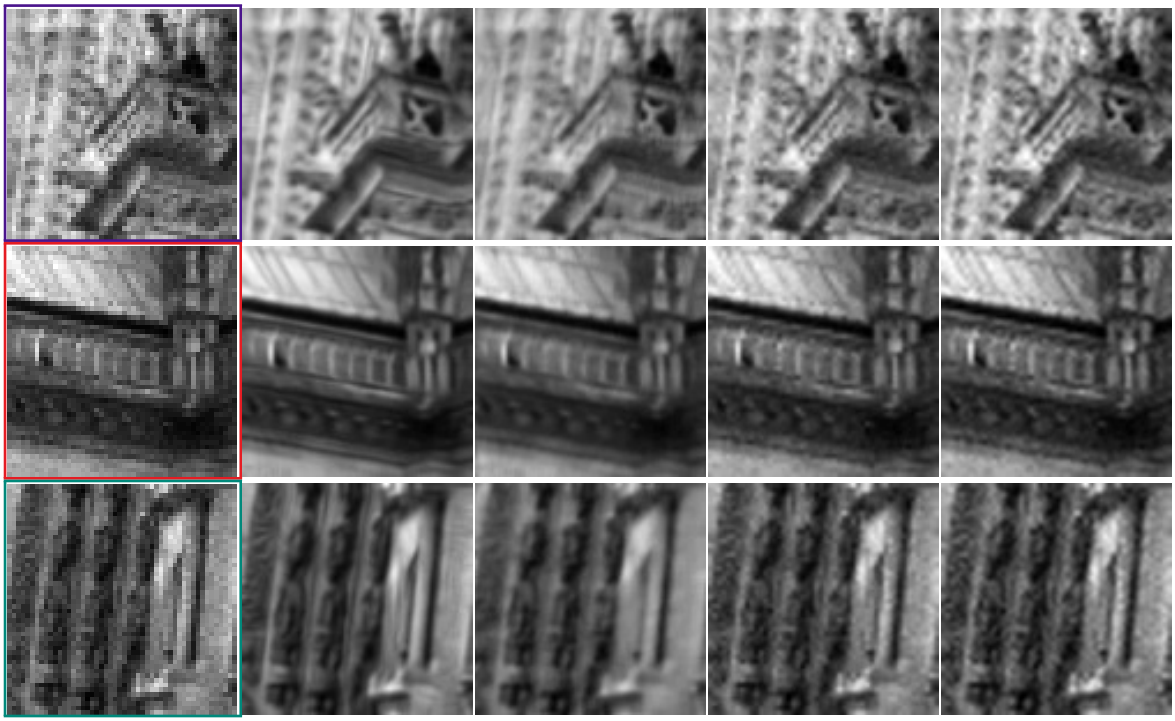

Fig. 6. **Real data. Zooming** $\times 2$**.** Interpolation of the green channel of a raw image (RGGB). **Left to right:** Input low-resolution image, result by HBE, PLEV [20], bicubic and lanczos interpolation.

The greatest advantage of this acquisition method is that it makes HDR imaging from a single image possible, thus avoiding the need for image alignment and motion estimation, which is the main drawback of the classical multi-image approach. Another advantage is that the saturated pixels are not organized in large regions. Indeed, some recent multi-image methods tackle the camera and objects motion problems by taking a reference image and then estimating motion relative to this frame or by recovering information from other frames through local comparison with the reference [27], [24]. A problem encountered by these approaches is the need to inpaint very large saturated and underexposed regions in the reference frame, since the information is completely lost in those areas. The SVE acquisition strategy avoids this problem since, in general, all scene regions are sampled by at least one of the exposures.

Taking advantage of the ability of the proposed framework to simultaneously estimate missing pixels and denoise well-exposed ones, we propose a novel approach to generate HDR images from a single shot acquired with spatially varying pixel exposures. The proposed approach shows significant improvements over existing approaches.

A. Spatially varying exposure acquisition model

As presented in [26], [28], [29], an optical mask with spatially varying transmittance can be placed adjacent to a conventional image sensor to give different exposure levels to the pixels. This optical mask does not change the acquisition process of the sensor, whether using a conventional CCD or CMOS sensor. Hence, the noise model (21) can be adapted to the SVE acquisition by including the per-pixel SVE gain o_p[4]

$$\mathrm{Z}(p) \sim \mathcal{N}(g o_p a_p \tau \mathrm{C}(p) + \mu_R, g^2 o_p a_p \tau \mathrm{C}(p) + \sigma_R^2). \quad (22)$$

In the approach proposed by Nayar and Mitsunaga [26], the varying exposures follow a regular pattern. Motivated by the aliasing problems of regular sampling patterns, Schöberl et al. [30] propose to use spatially varying exposures on a non-regular pattern. Figure 7 shows examples of both acquisition patterns. This fact led us to choose the non-regular pattern in the proposed approach.

B. Hyperprior Bayesian Estimator for Single Shot High Dynamic Range Imaging

1) Problem statement: In order to reconstruct the dynamic range of the scene we need to solve an inverse problem, that is, to find the irradiance values from the input pixel values. More precisely, we want to estimate the irradiance image C from the SVE image Z, knowing the exposure levels of the optical mask and the camera parameters.

For this purpose we map the raw pixel values to the irradiance domain Y with

$$\mathrm{Y}(p) = \frac{\mathrm{Z}(p) - \mu_R}{g o_p a_p \tau}. \quad (23)$$

We take into account the effect of saturation and under-exposure by introducing the exposure degradation matrix $\boldsymbol{D}$, a diagonal matrix given by

$$(\boldsymbol{D})_p = \begin{cases} 1 & \text{if } \mu_R < \mathrm{Z}(p) < z_{sat}, \\ 0 & \text{otherwise,} \end{cases} \quad (24)$$

[4]Some noise sources not modeled in [19], such as blooming, might have a considerable impact in the SVE acquisition strategy and should be considered in a more accurate image modeling.

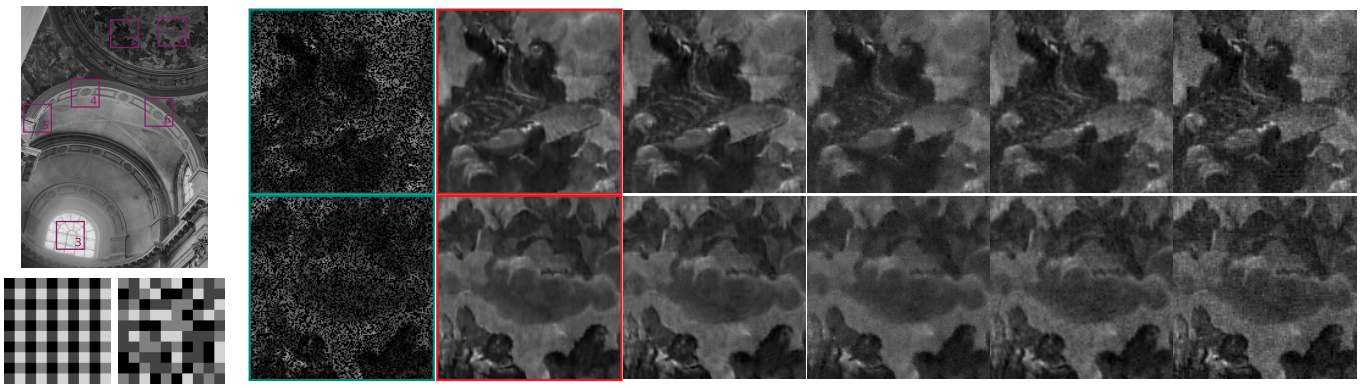

Fig. 7. **Synthetic data. Left:** (**top**) Tone mapped version of the ground-truth image used for the experiments in Section V-C1. Image from [31]. (**bottom**) Regular (left) and non-regular (right) optical masks for an example of 4 different filters. **Right:** Results for extracts 1 and 6. From left to right: Input image with random pattern, ground-truth, results by HBE, PLEV [20], Schöberl et al. [30], Nayar and Mitsunaga [26]. 50% missing pixels (for both random and regular pattern). See PSNR values for these extracts in Table II. Please see the digital copy for better details reproduction.

with z_{sat} equal to the pixel saturation value, thus eliminating the under or overexposed pixels. From (22) and (24), $\mathrm{Y}(p)$ can be modeled as

$$\mathrm{Y}(p)|(\boldsymbol{D})_p \sim \mathcal{N}\left((\boldsymbol{D})_p \mathrm{C}(p), \frac{g^2 o_p a_p \tau (\boldsymbol{D})_p \mathrm{C}(p) + \sigma_R^2}{(g o_p a_p \tau)^2}\right). \tag{25}$$

Notice that (25) is the distribution of $\mathrm{Y}(p)$ for a given exposure degradation factor $(\boldsymbol{D})_p$, since $(\boldsymbol{D})_p$ is itself a random variable that depends on $\mathrm{Z}(p)$. The exposure degradation factor must be included in (25) since the variance of the over or under exposed pixels no longer depends on the irradiance $\mathrm{C}(p)$ but is only due to the readout noise σ_R^2. From (25) we have

$$\mathrm{Y} = \boldsymbol{D}\mathrm{C} + \mathrm{N}, \tag{26}$$

where N is zero-mean Gaussian noise with diagonal covariance matrix $\boldsymbol{\Sigma}_{\mathrm{N}}$ given by

$$(\boldsymbol{\Sigma}_{\mathrm{N}})_j = \frac{g^2 o_p a_p \tau (\boldsymbol{D})_p \mathrm{C}(p) + \sigma_R^2}{(g o_p a_p \tau)^2}. \tag{27}$$

Then the problem of irradiance estimation can be stated as retrieving C from Y, which implies denoising the well-exposed pixel values ($(\boldsymbol{D})_p = 1$) and estimating the unknown ones ($(\boldsymbol{D})_p = 0$).

2) Proposed solution: From (26), image Y is under the hypothesis of the HBE framework so we can apply the proposed patch-based reconstruction approach to HDR imaging. The proposed HDR imaging algorithm consists of the following steps: **1)** generate $\boldsymbol{D}$ from Z according to (24), **2)** obtain Y from Z according to (23), **3)** apply the HBE approach to Y with the given $\boldsymbol{D}$ and $\boldsymbol{\Sigma}_{\mathrm{N}}$.

C. Experiments

The proposed reconstruction method was thoroughly tested in several synthetic and real data examples. A brief summary of the results is presented in this section.

1) Synthetic data: Sample images are generated according to Model (26) using the HDR image in Figure 7 as the ground-truth. Both a random and a regular pattern with four equiprobable exposure levels $o = \{1, 8, 64, 512\}$ are simulated. The exposure time is set to $\tau = 1/200$ seconds and the camera parameters are those of a Canon 7D camera set to ISO 200 ($g = 0.87$, $\sigma_R^2 = 30$, $\mu_R = 2048$, $\mathrm{v_{sat}} = 15000$) [19].

	PSNR (dB)					
	1 (Fig. 7)	2 (Fig. 7)	3	4	5	6
HBE	**33.08**	**33.87**	22.95	**35.10**	**36.80**	**35.66**
PLEV	29.65	30.82	22.77	33.99	36.42	34.73
Schöberl et al.	30.38	31.16	21.39	30.04	32.84	31.02
Nayar and Mitsunaga	29.39	30.10	**23.24**	25.83	30.26	26.90

TABLE II
PSNR VALUES FOR THE EXTRACTS SHOWN IN FIGURE 7.

Figure 7 shows extracts of the results obtained by the proposed method, by PLEV [20] and by Schöberl et al. [30] for the random pattern and by Nayar et Mitsunaga [26] using the regular pattern. The percentage of unknown pixels in the considered extracts is 50% (it is nearly the same for both the regular and non-regular pattern). Table II shows the PSNR values obtained in each extract marked in Figure 7. The proposed method manages to correctly reconstruct the irradiance on the unknown pixels. Moreover, its denoising performance is much better than that of Schöberl et al. and Nayar and Mitsunaga, but still sharper than PLEV.

2) Real data: The feasibility of the SVE random pattern has been shown in [29] and that of the SVE regular pattern in [28]. Nevertheless, these acquisition systems are still not available for general usage. However, as stated in Section V-A, the only variation between the classical and the SVE acquisition is the optical filter, i.e. the amount of light reaching each pixel. Hence, the noise at a pixel p captured using SVE with an optical gain factor o_p and exposure time τ/o_p and a pixel captured with a classical camera using exposure time τ should be very close. We take advantage of this fact in order to evaluate the reconstruction performance of the proposed approach using real data.

For this purpose, we generate an SVE image z_{sve} drawing pixels at random from four raw images $\{\mathrm{z}^i_{raw}\}_{i=1,\dots,4}$ acquired with different exposure times. The four different exposure times simulate four different filters of the SVE optical mask. More precisely, the value at position (x, y) in z_{sve} is chosen at random among the four available values at that

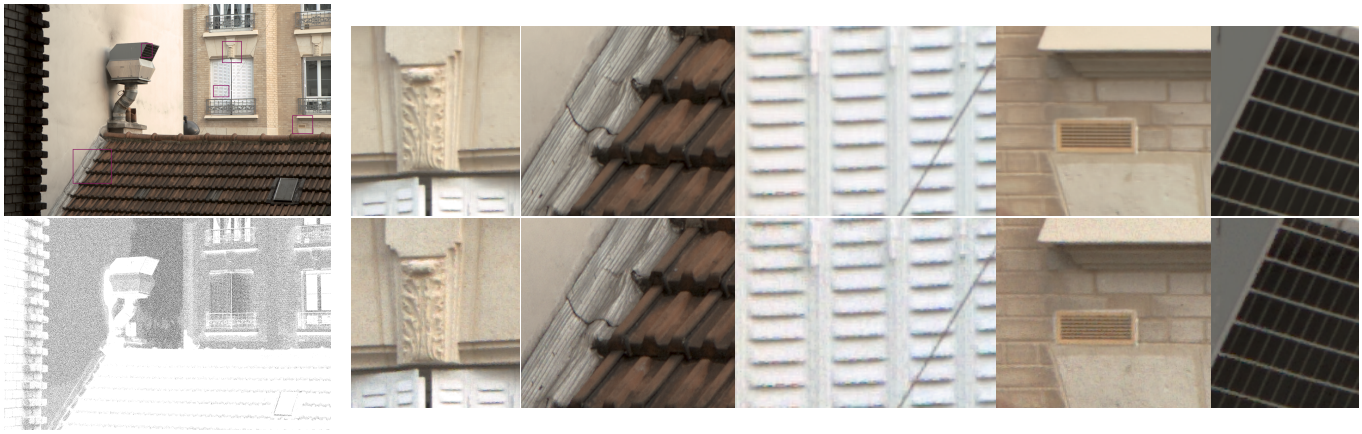

Fig. 8. **Real data. Left:** Tone mapped version of the HDR image obtained by the proposed approach and its corresponding mask of unknown (black) and well-exposed (white) pixels. **Right:** Comparison of the results obtained by the proposed approach (first row) and PLEV (second row) in the extracts indicated in the top image. Please see the digital copy for better details reproduction.

position $\{z^i_{raw}(x,y)\}_{i=1,\dots,4}$. Notice that the Bayer pattern is kept on z_{sve} by construction. The images $\{z^i_{raw}\}_{i=1,\dots,4}$ are acquired using a remotely controlled camera and a tripod so as to be perfectly aligned. Otherwise, artifacts may appear from the random sampling of the four images used to create the SVE frame.

This protocol does not allow us to take scenes with moving objects. Let us emphasize, however, that using a real SVE device, this, as well as the treatment of moving camera, would be a non-issue.

Figures 8 and 9 show the results obtained in two real scenes, together with the masks of well-exposed (white) and unknown (black) pixels. Recall that among the unknown pixels, some of them are saturated and some of them are under exposed pixels. Patch sizes 6 and 8 were used for the examples in Figure 9 and Figure 8 respectively. The demosaicking method by Adams and Hamilton [32] is then used to obtain a color image from the reconstructed irradiance. To display the results we use the tone mapping technique by Mantiuk et al. [33].

We compare the results to those obtained by PLEV. A comparison against the methods by Nayar and Mitsunaga and Schöberl et al. is not presented since they do not specify how to treat raw images with a Bayer pattern (how to treat color) and therefore an adaptation of their methods should be made in order to process our data. The proposed method manages to correctly reconstruct the unknown pixels even in extreme conditions where more than 70% of the pixels are missing, as for example the last extract in Figure 9.

These examples show the capacity of the proposed approach to reconstruct the irradiance information in both very dark and bright regions simultaneously. See for instance the example in Figure 9, where the dark interior of the building (which can be seen through the windows) and the highly illuminated part of another building are both correctly reconstructed (please consult the pdf version of this article for better visualization).

VI. Conclusions

In this work we have presented a novel image restoration framework. It has the benefits of local patch characterization proven suitable by the NLB denoising methods, but manages to extend its use to general restoration problems such as zooming, inpainting and interpolation, by combining local estimation with Bayesian restoration based on hyperpriors. In this way, all the restoration problems are set under the same framework. We have presented a large series of experiments on both synthetic and real data that confirm the robustness of the proposed strategy based on hyperpriors. These experiments show that for a wide range of image restoration problems HBE outperforms several state-of-the-art restoration methods.

This work opens several perspectives. The first one concerns the relevance of the Gaussian patch model and its relation to the underlying image patches manifold. If this linear approximation has proven successful for image restoration, its full relevance in other areas remains to be explored, especially in all domains requiring to compare image patches. Another important related question is the one of the estimation of the degradation model in images jointly degraded by noise, missing pixels, blur, etc. Restoration approaches generally rely on the precise knowledge of this model and of its parameters. In practice however, we often deal with images for which the acquisition process is unknown, and that have possibly been affected by post-treatments. In such cases, blind restoration remains an unsolved challenge.

Moreover, we have presented a novel application of the proposed general framework to the generation of HDR images from a single SVE snapshot. The SVE acquisition strategy allows the creation of HDR images from a single shot without the drawbacks of multi-image approaches, such as the need for global alignment and motion estimation to avoid ghosting problems. The proposed method manages to simultaneously denoise and reconstruct the missing pixels, even in the presence of (possibly complex) motions, improving the results obtained by existing methods. Examples with real data acquired in very similar conditions to those of the SVE acquisition show the capabilities of the proposed approach.

Fig. 9. **Real data. Left:** Tone mapped version of the HDR image obtained by the proposed approach and its corresponding mask of unknown (black) and well-exposed (white) pixels. **Right:** Comparison of the results obtained by the proposed approach (first row) and PLEV (second row) in the extracts indicated in the top image. Please see the digital copy for better details reproduction.

APPENDIX A
MAXIMUM A POSTERIORI ESTIMATION OF PARAMETERS

A. Patch model

The observed image z is decomposed into I overlapping patches $\{\mathrm{z}_i\}_{i=1,\dots,I}$ of size $\sqrt{n}\times\sqrt{n}$. Each patch $\mathrm{z}_i \in \mathbb{R}^{n\times 1}$ is considered to be a realization of the random variable Z_i given by

$$\mathrm{Z}_i = \boldsymbol{D}_i \mathrm{C}_i + \mathrm{N}_i, \tag{28}$$

where $\boldsymbol{D}_i \in \mathbb{R}^{n\times n}$ is a known degradation operator, $\mathrm{C}_i \in \mathbb{R}^{n\times 1}$ is the original patch we seek to estimate and $\mathrm{N}_i \in \mathbb{R}^{n\times 1}$ is an additive noise term. We assume a Gaussian prior for each patch, with unknown mean μ and covariance matrix $\boldsymbol{\Sigma}$

$$p(\mathrm{C}_i \mid \mu_i, \boldsymbol{\Sigma}_i) \sim \mathcal{N}(\mu_i, \boldsymbol{\Sigma}_i). \tag{29}$$

The additive noise term N_i is modeled by a Gaussian distribution $\mathrm{N}_i \sim \mathcal{N}(0, \boldsymbol{\Sigma}_{N_i})$. The matrix $\boldsymbol{\Sigma}_{N_i}$ is only assumed to be diagonal (the noise is uncorrelated). It can represent a constant variance, spatially variable variances or even variances dependent on the pixel value (to approximate Poisson noise). The distribution of Z_i given C_i can thus be written as

$$\begin{aligned} p(\mathrm{Z}_i \mid \mathrm{C}_i) &\sim \mathcal{N}(\boldsymbol{D}_i\mathrm{C}_i, \boldsymbol{\Sigma}_{N_i}) \\ &\propto |\boldsymbol{\Sigma}_{N_i}^{-1}|^{\frac{1}{2}} \exp\left(-\frac{1}{2}(\mathrm{Z}_i - \boldsymbol{D}_i\mathrm{C}_i)^T\boldsymbol{\Sigma}_{N_i}^{-1}(\mathrm{Z}_i - \boldsymbol{D}_i\mathrm{C}_i)\right). \end{aligned} \tag{30}$$

B. Unified maximum a posteriori

Let us consider a group $\{\mathrm{Z}_i\}_{i=1,\dots,M}$ of similar patches, from which we want to recover the restored patches $\{\mathrm{C}_i\}_{i=1,\dots,M}$. If these unknown $\{\mathrm{C}_i\}$ are independent and follow the same Gaussian model, we can compute the joint maximum a posteriori

$$\begin{aligned} &\underset{\{\mathrm{C}_i\},\mu,\boldsymbol{\Lambda}}{\arg\max}\ p(\{\mathrm{C}_i\},\mu,\boldsymbol{\Lambda} \mid \{\mathrm{Z}_i\}) = \\ &\underset{\{\mathrm{C}_i\},\mu,\boldsymbol{\Lambda}}{\arg\max}\ p(\{\mathrm{Z}_i\} \mid \{\mathrm{C}_i\},\mu,\boldsymbol{\Lambda})\ p(\{\mathrm{C}_i\} \mid \mu,\boldsymbol{\Lambda})\ p(\mu,\boldsymbol{\Lambda}) = \\ &\underset{\{\mathrm{C}_i\},\mu,\boldsymbol{\Lambda}}{\arg\max}\ p(\{\mathrm{Z}_i\} \mid \{\mathrm{C}_i\})\ p(\{\mathrm{C}_i\} \mid \mu,\boldsymbol{\Lambda})\ p(\mu,\boldsymbol{\Lambda}). \end{aligned} \tag{31}$$

In this product, the first term is given by the noise model (30), the second one is the Gaussian prior on the set of patches (29) and the third one is the Normal-Wishart hyperprior

$$\begin{aligned} p(\mu,\boldsymbol{\Lambda}) &= \mathcal{N}(\mu|\mu_0,(\kappa\boldsymbol{\Lambda})^{-1})\mathcal{W}(\boldsymbol{\Lambda}|(\nu\boldsymbol{\Sigma}_0)^{-1},\nu) \\ &\propto |\boldsymbol{\Lambda}|^{1/2}\exp\left(-\frac{\kappa}{2}(\mu-\mu_0)\boldsymbol{\Lambda}(\mu-\mu_0)^T\right) \\ &\quad |\boldsymbol{\Lambda}|^{(\nu-n-1)/2}\exp\left(-\frac{1}{2}\mathrm{tr}(\nu\boldsymbol{\Sigma}_0\boldsymbol{\Lambda})\right), \end{aligned} \tag{32}$$

where μ_0 is a prior on μ, $\boldsymbol{\Sigma}_0$ is a prior on $\boldsymbol{\Sigma}$, $\kappa > 0$ and $\nu > n-1$ are a scale parameter and the degrees of freedom of the Normal-Wishart respectively.

a) Maximization with respect to $\{\mathrm{C}_i\}$: If we ignore the dependence of $\boldsymbol{\Sigma}_{N_i}$ on C_i, we obtain

$$\frac{\partial \log p(\{\mathrm{C}_i\},\mu,\boldsymbol{\Lambda} \mid \{\mathrm{Z}_i\})}{\partial \mathrm{C}_i} = \boldsymbol{D}_i^T\boldsymbol{\Sigma}_{N_i}^{-1}(\mathrm{Z}_i - \boldsymbol{D}_i\mathrm{C}_i) - \boldsymbol{\Lambda}(\mathrm{C}_i - \mu). \tag{33}$$

Equating to zero, the solution is given by the Wiener estimator for each i separately

$$\mathrm{C}_i = \boldsymbol{\Lambda}^{-1}\boldsymbol{D}_i^T(\boldsymbol{D}_i\boldsymbol{\Lambda}^{-1}\boldsymbol{D}_i^T + \boldsymbol{\Sigma}_{N_i})^{-1}(\mathrm{Z}_i - \boldsymbol{D}_i\mu) + \mu. \tag{34}$$

b) Maximization with respect to μ: Derivating with respect to μ, we obtain

$$\frac{\partial \log p(\{\mathrm{C}_i\},\mu,\boldsymbol{\Lambda} \mid \{\mathrm{Z}_i\})}{\partial \mu} = \boldsymbol{\Lambda}\sum_{i=1}^{M}(\mu - \mathrm{C}_i) + \kappa\boldsymbol{\Lambda}(\mu - \mu_0), \tag{35}$$

which is zero if and only if (assuming $\boldsymbol{\Lambda}$ is invertible)

$$\mu = \frac{M\overline{C} + \kappa\mu_0}{M+\kappa}, \quad \text{with } \overline{C} = \frac{1}{M}\sum_{i=1}^{M}\mathrm{C}_i. \tag{36}$$

c) Maximization with respect to $\boldsymbol{\Lambda}$: The partial derivative with respect to $\boldsymbol{\Lambda}$ is slightly more complicated (see the Matrix

Cookbook for these derivations [34]). Observe that

$$\begin{aligned}\log p(\{\mathrm{C}_i\},\mu,\mathbf{\Lambda}\mid\{\mathrm{Z}_i\}) &= \frac{\nu-n+M}{2}\log|\mathbf{\Lambda}| \\ &- \frac{1}{2}\sum_{i=1}^{M}(\mathrm{C}_i-\mu)^T\mathbf{\Lambda}(\mathrm{C}_i-\mu) \\ &- \frac{\kappa}{2}(\mu-\mu_0)^T\mathbf{\Lambda}(\mu-\mu_0) \\ &- \frac{1}{2}\mathrm{trace}[\nu\mathbf{\Sigma}_0\mathbf{\Lambda}].\end{aligned} \tag{37}$$

The derivative of the first term is ($\mathbf{\Lambda}$ is symmetric)

$$\frac{\nu-n+M}{2}(\mathbf{\Lambda}^{-1})^T=\frac{\nu-n+M}{2}\mathbf{\Lambda}^{-1}.$$

The derivative of the second and third terms are

$$-\frac{1}{2}\sum_{i=1}^{M}(\mathrm{C}_i-\mu)(\mathrm{C}_i-\mu)^T$$

and

$$-\frac{\kappa}{2}(\mu-\mu_0)(\mu-\mu_0)^T.$$

Finally, the derivative of the fourth term is

$$-\frac{1}{2}\nu\mathbf{\Sigma}_0^T=-\frac{1}{2}\nu\mathbf{\Sigma}_0.$$

Then it follows that

$$\begin{aligned}\frac{\partial\log p(\{\mathrm{C}_i\},\mu,\mathbf{\Lambda}\mid\{\mathrm{Z}_i\})}{\partial\mathbf{\Lambda}} &= \frac{\nu-n+M}{2}\mathbf{\Lambda}^{-1} \\ &- \frac{1}{2}\sum_{i=1}^{M}(\mathrm{C}_i-\mu)(\mathrm{C}_i-\mu)^T \\ &- \frac{\kappa}{2}(\mu-\mu_0)(\mu-\mu_0)^T \\ &- \frac{1}{2}\nu\mathbf{\Sigma}_0.\end{aligned}$$

Equating to zero, this yields

$$\mathbf{\Lambda}^{-1}=\frac{\nu\mathbf{\Sigma}_0+\kappa(\mu-\mu_0)(\mu-\mu_0)^T+\sum_{i=1}^{M}(\mathrm{C}_i-\mu)(\mathrm{C}_i-\mu)^T}{\nu+M-n}. \tag{38}$$

d) Computation of the maximum in $\{\mathrm{C}_i\}$, μ and $\mathbf{\Lambda}$: If we inject the expression of the C_i's at the maximum into the previous expressions of μ and $\mathbf{\Lambda}$, we get

$$\begin{aligned}\mu &= \frac{M\overline{C}+\kappa\mu_0}{M+\kappa}, \\ &= \frac{\sum_{i=1}^{M}A_i(\mathrm{Z}_i-\boldsymbol{D}_i\mu)+M\mu+\kappa\mu_0}{M+\kappa},\end{aligned}$$

with $A_i=\mathbf{\Lambda}^{-1}\boldsymbol{D}_i^T(\boldsymbol{D}_i\mathbf{\Lambda}^{-1}\boldsymbol{D}_i^T+\mathbf{\Sigma}_{N_i})^{-1}$. Grouping all the terms in μ on the left hand side of the equation, we obtain

$$(\kappa\mathrm{Id}+\sum_{i=1}^{M}A_i\boldsymbol{D}_i)\mu=\sum_{i=1}^{M}A_i\mathrm{Z}_i+\kappa\mu_0. \tag{39}$$

In other words,

$$\mu=(\kappa\mathrm{Id}+\sum_{i=1}^{M}A_i\boldsymbol{D}_i)^{-1}(\sum_{i=1}^{M}A_i\mathrm{Z}_i+\kappa\mu_0). \tag{40}$$

In the same way, replacing the C_i's in (38) gives

$$\mathbf{\Lambda}^{-1}=\frac{1}{\nu+M-n}\Bigg(\nu\mathbf{\Sigma}_0+\kappa(\mu-\mu_0)(\mu-\mu_0)^T+ \tag{41}$$

$$\sum_{i=1}^{M}A_i(\mathrm{Z}_i-\boldsymbol{D}_i\mu)(\mathrm{Z}_i-\boldsymbol{D}_i\mu)^TA_i^T\Bigg). \tag{42}$$

Since Equations (40) and (42) depends both on $\mathbf{\Lambda}$ and μ, we cannot obtain closed forms for the values of μ and $\mathbf{\Lambda}$ at the maximum. These two equations can however be seen as a fixed point problem. In practice, we use an iterative approach to find the values of μ and $\mathbf{\Lambda}$ from Equations (40) and (42), followed by Equation (34) to restore the patches.

C. Affine risk minimizer

Proposition 3. *Assume that the noise has zero mean and is not correlated to the signal C_i. Then, the affine estimator $\tilde{\mathrm{C}}_i$ that minimizes the Bayes risk $\mathbb{E}[(\tilde{\mathrm{C}}_i-\mathrm{C}_i)^2]$ is given by*

$$\tilde{\mathrm{C}}_i=\mathbf{\Lambda}^{-1}\boldsymbol{D}_i^T(\boldsymbol{D}_i\mathbf{\Lambda}^{-1}\boldsymbol{D}_i^T+\mathbf{\Sigma}_{\mathrm{N}_i})^{-1}(\mathrm{Z}_i-\boldsymbol{D}_i\mu)+\mu. \tag{43}$$

Proof. Let us first consider the case $\mu=0$. If we consider linear estimators only, we look for the matrix $\tilde{\mathbf{W}}$ that verifies

$$\tilde{\mathbf{W}}=\arg\min_{\mathbf{W}}\mathbb{E}[(\mathbf{W}\mathrm{Z}_i-\mathrm{C}_i)^2]. \tag{44}$$

Hence, $\tilde{\mathbf{W}}$ must verify

$$\mathbb{E}[(\tilde{\mathbf{W}}\mathrm{Z}_i-\mathrm{C}_i)\mathrm{Z}_i^T]=0, \tag{45}$$

and we have

$$\tilde{\mathbf{W}}=\mathbb{E}[\mathrm{C}_i\mathrm{Z}_i^T](\mathbb{E}[\mathrm{Z}_i\mathrm{Z}_i^T])^{-1}. \tag{46}$$

Since the noise N_i has zero mean and is not correlated to the signal C_i, the element (p,q) of matrix $\mathbb{E}[\mathrm{C}_i\mathrm{Z}_i^T]$ is given by

$$\begin{aligned}\mathbb{E}[\mathrm{C}_i\mathrm{Z}_i^T]_{p,q} &= \mathbb{E}[\mathrm{C}_i(\boldsymbol{D}_i\mathrm{C}_i+\mathrm{N}_i)^T]_{p,q} &(47)\\ &= \mathbb{E}[\mathrm{C}_i^p(\boldsymbol{D}_i\mathrm{C}_i)_q+\mathrm{C}_i^p\mathrm{N}_i^q] &(48)\\ &= (\mathbf{\Lambda}^{-1}\boldsymbol{D}_i^T)_{p,q}. &(49)\end{aligned}$$

Also, the element (p,q) of matrix $\mathbb{E}[\mathrm{Z}_i\mathrm{Z}_i^T]$ is given by

$$\begin{aligned}\mathbb{E}[\mathrm{Z}_i\mathrm{Z}_i^T]_{p,q} &= \mathbb{E}[(\boldsymbol{D}_i\mathrm{C}_i+\mathrm{N}_i)(\boldsymbol{D}_i\mathrm{C}_i+\mathrm{N}_i)^T]_{p,q} &(50)\\ &= \mathbb{E}[(\boldsymbol{D}_i\mathrm{C}_i)_p(\boldsymbol{D}_i\mathrm{C}_i)_q^T+(\boldsymbol{D}_i\mathrm{C}_i)_p(\mathrm{N}_i)_q^T &(51)\\ &\quad+(\mathrm{N}_i)_p(\boldsymbol{D}_i\mathrm{C}_i)_q+(\mathrm{N}_i)_p(\mathrm{N}_i)_q^T] &(52)\\ &= (\boldsymbol{D}_i\mathbf{\Lambda}^{-1}\boldsymbol{D}_i^T)_{p,q}+(\mathbf{\Sigma}_{\mathrm{N}_i})_{p,q}. &(53)\end{aligned}$$

Hence we have,

$$\tilde{\mathbf{W}}=\mathbf{\Lambda}^{-1}\boldsymbol{D}_i^T(\boldsymbol{D}_i\mathbf{\Lambda}^{-1}\boldsymbol{D}_i^T+\mathbf{\Sigma}_{\mathrm{N}_i})^{-1}. \tag{54}$$

In the general case where $\mu\neq0$, we can always consider the centered version of the patches $(Z_i-\boldsymbol{D}_i\mu)$ and apply the previous result. Therefore, the estimator of C_i that minimizes the risk function $\mathbb{E}[(\tilde{\mathrm{C}}-\mathrm{C}_i)^2]$ among all affine estimators under Model (28), is given by (43). □

ACKNOWLEDGMENT

The authors would like to thank the authors of [18], [12] and [17] of for kindly providing their code. This work has been partially funded by the French Research Agency (ANR) under grant nro ANR-14-CE27-001 (MIRIAM).

REFERENCES

[1] H. Maître, *From Photon to Pixel: The Digital Camera Handbook*. Wiley, 2016.

[2] A. A. Efros and T. K. Leung, "Texture Synthesis by Non-Parametric Sampling," in *Proc. IEEE Int. Conf. Comput. Vis. (ICCV)*, 1999, pp. 1033–1038.

[3] A. Buades, B. Coll, and J. M. Morel, "A Review of Image Denoising Algorithms, with a New One," *Multiscale Model. Simul.*, vol. 4, no. 2, pp. 490–530, 2005.

[4] S. Lyu and E. Simoncelli, "Modeling Multiscale Subbands of Photographic Images with Fields of Gaussian Scale Mixtures," *IEEE Pattern Anal.*, vol. 31, no. 4, pp. 693–706, 2009.

[5] P. Chatterjee and P. Milanfar, "Patch-Based Near-Optimal Image Denoising," *IEEE Trans. Image Process.*, vol. 21, no. 4, pp. 1635–1649, 2012.

[6] M. Lebrun, A. Buades, and J. Morel, "A nonlocal bayesian image denoising algorithm," *SIAM J Imaging Sci*, vol. 6, no. 3, pp. 1665–1688, 2013.

[7] Y.-Q. Wang and J.-M. Morel, "SURE Guided Gaussian Mixture Image Denoising," *SIAM J Imaging Sci*, vol. 6, no. 2, pp. 999–1034, 2013.

[8] D. Zoran and Y. Weiss, "From learning models of natural image patches to whole image restoration," in *Proc. IEEE Int. Conf. Comput. Vis. (ICCV)*, 2011, pp. 479–486.

[9] G. Yu, G. Sapiro, and S. Mallat, "Solving inverse problems with piecewise linear estimators: From gaussian mixture models to structured sparsity," *IEEE Trans. Image Process.*, vol. 21, no. 5, pp. 2481–2499, 2012.

[10] M. Lebrun, M. Colom, A. Buades, and J. Morel, "Secrets of image denoising cuisine," *Acta Numerica*, vol. 21, no. 1, pp. 475–576, 2012.

[11] Y.-Q. Wang, "The Implementation of SURE Guided Piecewise Linear Image Denoising," *Image Processing On Line*, vol. 3, pp. 43–67, 2013.

[12] ——, "E-PLE: an Algorithm for Image Inpainting," *Image Processing On Line*, vol. 2013, pp. 271–285, 2013.

[13] H. Raiffa and R. Schlaifer, *Applied statistical decision theory*. Division of Research, Graduate School of Business Administration, Harvard University Boston, 1961.

[14] C. Aguerrebere, J. Delon, Y. Gousseau, and P. Musé, "Study of the digital camera acquisition process and statistical modeling of the sensor raw data," *Technical report hal-00733538v1*, 2012.

[15] P. Arias, V. Caselles, and G. Facciolo, "Analysis of a Variational Framework for Exemplar-Based Image Inpainting," *Multiscale Model. Simul.*, vol. 10, no. 2, pp. 473–514, 2012.

[16] K. Dabov, A. Foi, V. Katkovnik, and K. Egiazarian, "Image denoising by sparse 3d transform-domain collaborative filtering," *IEEE Trans. Image Process.*, vol. 16, no. 8, 2007.

[17] D. Zoran and Y. Weiss, "From learning models of natural image patches to whole image restoration," http://people.csail.mit.edu/danielzoran/epllcode.zip, accessed: 29/09/2014.

[18] M. Lebrun, A. Buades, and J.-M. Morel, "Implementation of the "Non-Local Bayes" (NL-Bayes) Image Denoising Algorithm," *Image Processing On Line*, vol. 3, pp. 1–42, 2013.

[19] C. Aguerrebere, J. Delon, Y. Gousseau, and P. Mus, "Best Algorithms for HDR Image Generation. A Study of Performance Bounds," *SIAM J Imaging Sci*, vol. 7, no. 1, pp. 1–34, 2014.

[20] C. Aguerrebere, A. Almansa, J. Delon, Y. Gousseau, and P. Muse, "Single shot high dynamic range imaging using piecewise linear estimators," in *Proc. IEEE Int. Conf. Comput. Phot. Pattern Recog. (ICCP)*, 2014.

[21] A. Buades, B. Coll, and J.-M. Morel, "Non-Local Means Denoising," *Image Processing On Line*, vol. 1, 2011.

[22] P. E. Debevec and J. Malik, "Recovering High Dynamic Range Radiance Maps from Photographs," in *COMP GRAPH*, 1997, pp. 369–378.

[23] M. Granados, B. Ajdin, M. Wand, C. Theobalt, H. P. Seidel, and H. P. A. Lensch, "Optimal HDR reconstruction with linear digital cameras," in *Proc. IEEE Conf. Comput. Vis. Pattern Recog. (CVPR)*, 2010, pp. 215–222.

[24] C. Aguerrebere, J. Delon, Y. Gousseau, and P. Muse, "Simultaneous HDR image reconstruction and denoising for dynamic scenes," in *Proc. IEEE Int. Conf. Comput. Phot. Pattern Recog. (ICCP)*, 2013, pp. 1–11.

[25] D. Sidibé, W. Puech, and O. Strauss, "Ghost detection and removal in high dynamic range images," in *Proc. European Signal Process. Conf.*, 2009.

[26] S. Nayar and T. Mitsunaga, "High Dynamic Range Imaging: Spatially Varying Pixel Exposures," in *Proc. IEEE Conf. Comput. Vis. Pattern Recog. (CVPR)*, vol. 1, Jun 2000, pp. 472–479.

[27] P. Sen, N. K. Kalantari, M. Yaesoubi, S. Darabi, D. B. Goldman, and E. Shechtman, "Robust patch-based HDR reconstruction of dynamic scenes," *ACM Transactions on Graphics*, vol. 31, no. 6, pp. 203:1–203:11, 2012.

[28] F. Yasuma, T. Mitsunaga, D. Iso, and S. Nayar, "Generalized Assorted Pixel Camera: Post-Capture Control of Resolution, Dynamic Range and Spectrum," *IEEE Trans. Image Process.*, vol. 99, Mar 2010.

[29] M. Schöberl, A. Belz, A. Nowak, J. Seiler, A. Kaup, and S. Foessel, "Building a high dynamic range video sensor with spatially nonregular optical filtering," in *Proc. SPIE Appl. Digital Image Process*, 2012, pp. 84 990C–84 990C–11.

[30] M. Schöberl, A. Belz, J. Seiler, S. Foessel, and A. Kaup, "High dynamic range video by spatially non-regular optical filtering," in *Proc. IEEE Image Proc (ICCP)*, 2012, pp. 2757–2760.

[31] S. Hasinoff, F. Durand, and W. Freeman, "Noise-optimal capture for high dynamic range photography," http://people.csail.mit.edu/hasinoff/hdrnoise/, last accessed: 17/03/2014.

[32] J. Hamilton and J. Adams, "Adaptive color plan interpolation in single sensor color electronic camera," US Patent 5,629,734, 1997.

[33] R. Mantiuk, S. Daly, and L. Kerofsky, "Display adaptive tone mapping," *ACM Transactions on Graphics*, vol. 27, no. 3, pp. 68:1–68:10, 2008.

[34] K. B. Petersen and M. S. Pedersen, "The matrix cookbook," Technical University of Denmark, Tech. Rep., 2012.